State-dependent effects of natural forcing on global and local climate variability

Beatrice Ellerhoff[1], Moritz Johannes Kirschner[2], Elisa Ziegler[3], Max Daniel Holloway[4], Louise C Sime[4], and Kira Rehfeld[3]

[1]Geo- and Environmental Research Center, Universität Tübingen
[2]Institute of Environmental Physics
[3]Geo- and Environmental Research Center
[4]British Antarctic Survey

November 26, 2022

Abstract

Natural forcing from solar and volcanic activity contributes significantly to climate variability. The post-eruption cooling of strong volcanic eruptions was hypothesized to have led to millennial-scale variability in the Glacial and to be weakened in warmer climate states. The underlying question is whether the climatic response to natural forcing is state-dependent. Here, we quantify the response to natural forcing under Last Glacial and Pre-Industrial conditions in an ensemble of climate model simulations. We evaluate internal and forced variability on annual to multicentennial scales. The global temperature response reveals no state dependency. Findings on the ability of models to simulate past variability could therefore translate to future climates. Small local differences result mainly from state-dependent sea ice changes. Variability in forced simulations matches paleoclimate reconstructions significantly better than in unforced scenarios. Considering natural forcing is therefore important for model-data comparison and future projections.

State-dependent effects of natural forcing on global and local climate variability

Beatrice Ellerhoff[1,2,3], Moritz J. Kirschner[1], Elisa Ziegler[1,2,3], Max D. Holloway[4], Louise Sime[5], Kira Rehfeld[1,2,3]

[1]Institute of Environmental Physics, Heidelberg, Germany
[2]Department of Physics and Department of Geoscience, Tübingen University, Tübingen, Germany
[3]Geo- und Umweltforschungszentrum, Tübingen University, Tübingen, Germany
[4]Scottish Association for Marine Science, Oban, United Kingdom
[5]British Antarctic Survey, Cambridge, United Kingdom

Key Points:

- We present Glacial/Interglacial climate simulations and quantify effects of time-varying volcanic and solar forcing on climate variability
- The mean global and local response to these forcings is similar in Glacial and Interglacial climate, suggesting a weak state dependency
- In both climate states, modeled temperature variance agrees better with palaeoclimate data when volcanic and solar forcing is included

Corresponding author: Kira Rehfeld, `kira.rehfeld@uni-tuebingen.de`

Abstract

Natural forcing from solar and volcanic activity contributes significantly to climate variability. The post-eruption cooling of strong volcanic eruptions was hypothesized to have led to millennial-scale variability in the Glacial and to be weakened in warmer climate states. The underlying question is whether the climatic response to natural forcing is state-dependent. Here, we quantify the response to natural forcing under Last Glacial and Pre-Industrial conditions in an ensemble of climate model simulations. We evaluate internal and forced variability on annual to multicentennial scales. The global temperature response reveals no state dependency. Findings on the ability of models to simulate past variability could therefore translate to future climates. Small local differences result mainly from state-dependent sea ice changes. Variability in forced simulations matches paleoclimate reconstructions significantly better than in unforced scenarios. Considering natural forcing is therefore important for model-data comparison and future projections.

Plain Language Summary

Climate variability describes the spatial and temporal variations of Earth's climate. It is a key factor influencing extreme weather events. Yet, it is unclear whether these variations depend on the mean surface temperature of the Earth or not. Here, we investigate the effects of natural forcing from volcanic eruptions and solar activity changes on climate variability. We compare simulations of a past (cold) and present (warm) climate with and without volcanism and solar changes. We find that overall, the climate system responds similarly to natural forcing in the cold and warm state. Small local differences mainly occur where ice can form. To evaluate the simulated variability, we use data from paleoclimate archives, including trees, ice-cores, and marine sediments. Climate variability from forced simulations agrees better with the temperature variability obtained from data. Natural forcing is therefore critical for reliable simulation of variability in past and future climates.

1 Introduction

Climate variability, that is variations in the statistics of climate parameters, characterizes Earth's dynamical system and is the primary influence on extreme events (Katz & Brown, 1992). Variability arises from unforced processes, internal to the climate system, and from forced processes, caused by external natural and anthropogenic drivers. Natural drivers include volcanic and solar forcing, contributing significantly to climate variability (Crowley, 2000). Due to anthropogenic activities, the recent trend of global mean surface temperature (GMST) and other variables has clearly emerged beyond the range of natural variability (Bindoff et al., 2013; Hasselmann, 1997; Marcott et al., 2013; Sippel et al., 2020).

Global warming also affects climate variability (Bathiany et al., 2018; Olonscheck et al., 2021). The underlying mechanisms remain poorly understood. There is conflicting and incomplete evidence on the spatio-temporal patterns of change (Brown et al., 2017; Holmes et al., 2016; Rehfeld et al., 2020; Pendergrass et al., 2017; Huntingford et al., 2013). This is a major source of uncertainty for regional climate projections. The abilities of models to accurately simulate climate variability requires that they resolve internal variability and the response to natural forcing across scales and mean climate states (Rehfeld et al., 2018).

Large explosive volcanic eruptions are suggested to have driven millennial-scale climate variations during glacial periods (Baldini et al., 2015). The largest eruption was hypothesized to have caused a human population bottleneck (Ambrose, 1998). The extent and impact of this event remains unclear (Timmreck et al., 2010; Svensson et al., 2013). Strong tropical volcanic eruptions have also been shown to influence daily temperature and precipitation extremes (T. Wang et al., 2021). These eruptions are hypothesized to induce a somewhat weaker response in warmer climates (Hopcroft et al., 2018), but volcanism will continue to play an important role in future variability (Bethke et al., 2017). These studies, however, do not examine the dependency of forced variability on the mean climate because they rely on future projections or the responses to large eruptions.

The paleoclimate record is crucial to assess whether a colder planet is more sensitive to natural forcing than a warmer one. Yet, temperature variability shows a mismatch between paleoclimate simulations and proxy data on the decadal-to-multicentennial scale (Laepple & Huybers, 2014a; Ellerhoff & Rehfeld, 2021). Paleoclimate simulations for the Last Glacial Maximum (LGM) or Pre-Industrial (PI) have mostly been performed without high frequency solar and volcanic forcing (Braconnot et al., 2012; Kageyama et al., 2018). This lack could potentially explain the mismatch between reconstructed and simulated variability. Additional uncertainty remains about the mechanisms of local, long-term variability (Franzke et al., 2020; Huybers & Curry, 2006; Fredriksen & Rypdal, 2017).

Separating internal and external variability has improved the understanding of climate dynamics and its underlying mechanisms (Schurer et al., 2013; Haustein et al., 2019; Frankcombe et al., 2015; Mann et al., 2022). Such an approach could also allow to identify drivers of local, decadal-to-multicentennial variability in cold and warm climates. This requires the comparison of unforced and forced climate simulations under Glacial and Interglacial conditions, and their validation against paleoclimate data over a wide range of timescales. There is also a need to study contributions to surface climate variability of system components that bridge internal and external factors. Sea ice, for example, follows in extent the mean state. Natural forcing could, however, also drive the multidecadal variability of sea ice extent via modulation of the Atlantic Meridional Overturning Circulation (AMOC) (Halloran et al., 2020). This highlights the need to study the contribution to variability from climate components and mechanisms that bridge intrinsic and external factors.

Here, we contrast unforced and naturally forced simulations under LGM and PI conditions in an ensemble using the Hadley Centre Coupled Model Version 3.4 (HadCM3; (Gordon et al., 2000; Pope et al., 2000; Stott et al., 2000; Reichler & Kim, 2008)). We examine the mean local response of the surface climate to volcanism in the two climate states (section 3.1). Spectral analysis (section 3.2) further quantifies the state- and timescale-dependent effects of natural forcing on local, zonal, and global scales. It confirms a robust response to natural forcing across climate states, but a mean decline in local temperature variability with warming. To aid interpretation of the spectra, we investigate sea ice dynamics as it appears a main contributor to local, long-term variability. We validate simulated variances using proxy data (section 3.3) to confirm that the addition of natural forcing significantly reduces the model-data mismatch on multidecadal and longer timescales. Thus, the inclusion of natural forcing provides a more accurate representation of climate variability, needed for climate simulations.

2 Data and Methods

2.1 Model Setup

Our simulation ensemble consists of 12 unforced and forced runs using LGM or PI boundary conditions (Table S1, Figure S1 in Supporting Information S1). We performed the simulations using HadCM3, a three-dimensional, coupled atmosphere-ocean general circulation model (AOGCM) that has been widely used for paleoclimate study (Valdes et al., 2017; Tindall et al., 2009; Flato et al., 2014; Reichler & Kim, 2008; Collins et al., 2001; Armstrong et al., 2022; Bühler et al., 2021). Despite its comparatively low resolution, HadCM3's simulated climate is comparable to other AOGCMs and observations

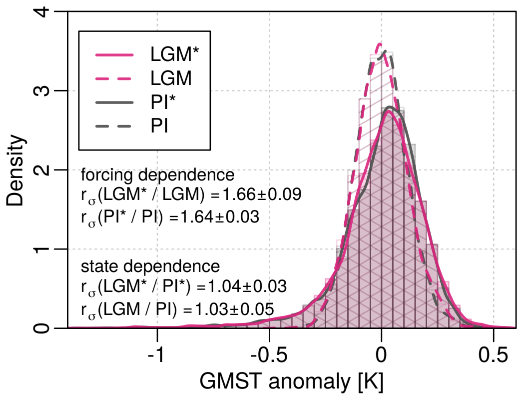

Figure 1. Distribution of simulated yearly GMST anomalies from all Pre-Industrial (PI) and Last Glacial Maximum (LGM) runs. Forced scenarios are marked with a (*). The ratio of the distributions' standard deviations is given by r_σ.

(Gordon et al., 2000; Jackson & Vellinga, 2013). The computational efficiency of HadCM3 allows for longterm integrations and ensemble comparisons.

The simulations are monthly resolved and of millennial length. The boundary conditions (orography, orbital parameters, greenhouse gas concentrations) define the mean state and are held constant over these runs. All runs start from the same LGM/PI spin-up simulation at consecutive years. Temperature, precipitation, sea level pressure, and wind fields are shown in Figure S2. The Last Glacial GMST is decidedly colder $(9.5 \pm 1.4)\,°\mathrm{C}$ and the global mean precipitation rate (GMPR) is lower $(935 \pm 20)\,\mathrm{mm\,yr^{-1}}$, with a steeper equator-to-pole temperature gradient than the Pre-Industrial with $(15.1 \pm 1.3)\,°\mathrm{C}$ and $(1048 \pm 21)\,\mathrm{mm\,yr^{-1}}$, respectively.

To facilitate comparison between climate variability in the LGM and PI, we apply the same transient volcanic and solar forcing (Figure S1), following the PMIP3 protocol (Schmidt et al., 2012). The forcing is updated every ten days in the model simulation. The time series prescribing the total solar irradiance consists of data from Steinhilber et al. (2009) and Y. Wang et al. (2005), with a superposed 11-year cycle (Schmidt et al., 2012). For volcanic forcing, we use the eruption reconstruction from Crowley and Unterman (2013). We supply the Aerosol Optical Depth (AOD) time series defined at a wavelength of 0.55μm which is converted into an aerosol mass loading factor (Crowley & Unterman, 2013; Schmidt et al., 2012). Three runs exist for each state and each forcing scenario (Table S2). Unless otherwise specified, our results represent average values of these sub-ensembles.

Figure 1 shows the distribution of simulated global mean surface temperature anomalies for the Last Glacial and Pre-Industrial. Forced scenarios are marked with a star (*) and exhibit larger fluctuations. The GMST standard deviation is increased by a factor of approximately 1.65 compared to unforced runs. By contrast, there is no major difference in the GMST distribution attributable to the mean climate.

2.2 Observations and Paleoclimate Reconstructions

We use observations and paleoclimate reconstructions to validate the variance from model simulation on interannual to multicentennial scales (2-5, 5-50, 50-200, and 200-500 years). We consider proxy records from Rehfeld et al. (2018), and the PAGES2k-Consortium (2017), and observations from the Met Office Hadley Centre's sea surface temperature dataset (HadISST downloaded 11/2019; (Rayner et al., 2003)). We focus on sea surface temperatures to facilitate comparison with proxy data, mainly stemming from ocean sites. We select records that (1) are published and calibrated to temperature, (2) consist of more than 50 data points, (3) cover at least three times the largest period of interest, and (4) have a mean sampling frequency of twice the highest frequency considered (Ellerhoff & Rehfeld, 2021). We exclude proxy records with gaps larger than five times the required resolution. Ice core records are not considered on timescales below 50 years, where signal-to-noise ratios are low (Laepple et al., 2018; Casado et al., 2020). Our ensemble consists of 41 observations and 115 proxy records from six different archives. The separately uploaded dataset (supporting information S2) lists the considered data. Figures S10 and S11 display their power spectra.

2.3 Effect Analysis

We analyze the global and local state-dependent effects of natural forcing in time and spectral domain. Following Swingedouw et al. (2017), we quantify local climate effects of moderate to large-magnitude volcanic eruptions using the mean standardized anomaly (MSA). The MSA is computed for 12-month means surrounding periods with high aerosol imprint (AOD $>$ 0.13, corresponding to approx. -2.6 W/m^2 (Forster et al., 2021)) as follows

$$\mathrm{MSA} = \frac{1}{j} \sum_j \frac{\frac{1}{12} \sum_{i \in T_j} X_i - \mu}{\sigma}\,, \tag{1}$$

with mean $\mu = \mathrm{E}[X]$ and standard deviation $\sigma = \sqrt{\mathrm{E}[(X-\mu)^2]}$ of each gridbox time series X. The index i specifies the 12 months of the time series X corresponding to the set of periods T_j for run j of each climate state. The normalization to the local variability σ allows detecting forced variations caused by volcanic eruptions. We test for statistical significance by bootstrapping using 400 block samples of X with a fixed length of 48 months.

We quantify the timescale-dependent variance of surface air temperature using the power spectral density (PSD, denoted spectrum). We obtain the spectrum applying the multitaper method (Percival & Walden, 1993) with three windows and chi-square distributed uncertainties. The required assumption of weak stationarity (Davies & Chatfield, 1990) is reasonably fulfilled, given that we linearly detrend all time series (Nilsen et al., 2016; Fredriksen & Rypdal, 2016; Laepple & Huybers, 2014b). We logarithmically smooth the spectra using a Gaussian kernel of 0.02 decibels. Following Huybers and Curry (2006), we compute mean spectra after interpolation to the lowest resolution and binning into equally spaced log-frequency intervals.

We use variance ratios, as in Laepple and Huybers (2014b), Rehfeld et al. (2018) and Ellerhoff and Rehfeld (2021), to compare the variance between model simulations and observational data. We first interpolate the observation and proxy data onto an equidistant time axis, using the same mean resolution as the raw signal. We compute the spectrum and obtain the variance by integration over the considered timescale (2-5, 5-20, 50-200, 200-500 years). Finally, we calculate the variance ratio by dividing the simulated by the reconstructed variance. Confidence intervals are obtained from a F-distribution, based on the degrees of freedom of the variance estimates. For the longest timescale (200-500 years), the “lgm3” and “pi2” run (Table S2) are excluded due to their comparatively short coverage. The change in variance ratios between forced and unforced runs is quantified by the area-weighted mean of the improvement factor (Appendix A).

3 Results

3.1 Mean Response to Volcanic Forcing

Volcanic eruptions cause mean temperature decline at almost every location (Fig. 2 (a) and (b)) as expected (Robock, 2000). The mean response, quantified by MSA, is weaker over the oceans than over land. Moreover, the response is stronger between 30°N and 30°S than in high-latitude regions, largely following the mean AOD imprint (Fig. 2 (c)). The strongest cooling (up to three standard deviations) occurs over the Southeast Asian Archipelago (Fig. 2 (b)). These patterns are largely robust against changes in the mean climate. This also applies to precipitation, sea level pressure, and 500mbar wind speed (Figure S3).

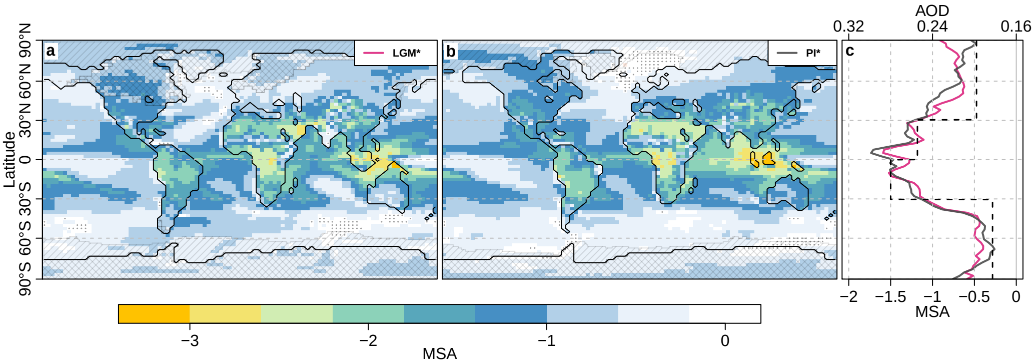

Figure 2. **a** Mean standardized anomalies (MSA) of surface air temperature in the LGM* **b** and the PI* state after volcanic eruptions. Dots indicate insignificant anomalies within the 99% quantile range of local variability. Grey shaded crosses show land ice. Hatched areas indicate areas with >50% yearly sea ice coverage. **c** Zonally averaged MSA and Aerosol Optical Depth (AOD) (black dashed).

The zonally averaged MSA (Fig. 2 (c)) reveals small differences between the states during LGM* and PI* around the equator, 60°S, 50°N, and towards the North Pole. We identify corresponding differences in Southeast Asia, the Antarctic Ocean, over the Northern Hemisphere (NH) ice sheets, and the Barents Sea (Fig. 2 (a) and (b)). In Southeast Asia, the enhanced PI* surface climate response could be linked to the high AOD imprint from strong tropical volcanic eruptions (Fasullo et al., 2017), such as the 1257 Samalas eruption. This region also features significant changes in the land-sea mask, which alter the local coupling between ocean and surface climate. In the Last Glacial, the cooling in response to volcanism is enhanced at the Antarctic sea ice edge and in the Barents Sea. Both regions feature a much higher amount of sea ice cover during the Last Glacial. The variations in MSA extend towards the Arctic Ocean and Northern North Atlantic. Differences between the states could therefore be related to the potential for sea ice formation, likely amplifying the local response to volcanic eruptions (Timmreck, 2012). Remaining small differences are found in regions with state-dependent changes of Northern Hemisphere (NH) ice sheets, with a tendency towards enhanced cooling over NH land masses in the Pre-Industrial.

3.2 Spectral Response at the Global and Local Scale

Examining power spectra for the global and local scale highlights the timescale-dependent impact of natural forcing. Global mean spectra of simulated temperatures (Fig. 3

(a)) are predominately determined by natural forcing. Including the forcing increases the power, and thus variance, on all timescales. At multidecadal scales, the forced GMST shows approximately five times more variance than unforced runs. State-dependent effects of the forced response are not discernible in these spectra.

Local mean spectra (Fig. 3 (a)) are characteristic for the mean state and less affected by natural forcing. They point to a greater temperature variance during the Last Glacial. Differences between the states are the strongest on interannual scales, where LGM$^{(*)}$ variance is increased by a factor of approximately two compared to PI$^{(*)}$. Zonal mean spectra (Fig. 3 (b) and (c)) reveal that the decrease in variability with warming is greatest at mid-, and especially high-latitudes, supporting a potential link to sea ice dynamics. The tropical variability widely agrees across states. Differences between forced and unforced local and zonal mean spectra are within uncertainties, but most pronounced for high-latitude, long-term variability.

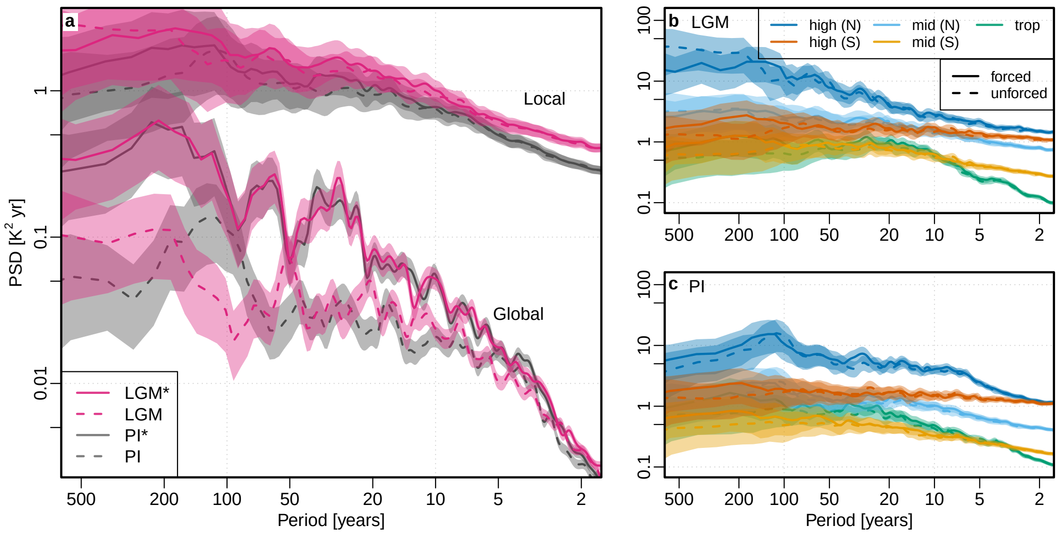

Figure 3. **a** Local (top) and global (bottom) PSD for simulated temperature using HadCM3. Global spectra are computed from the global mean surface temperature. Local refers to the area-weighted average of all local spectra. **b** and **c** Area-weighted average of local spectra by climate zone, given by the tropics (-23.5 to 23.5 °N), mid (23.5 to 66.5°), and high latitudes (>66.5°) for LGM and PI. Lines show the logarithmically smoothed mean spectrum, with shaded 95% confidence intervals.

3.3 Comparison of Observed and Modeled Variability

We validate the simulated variability against observational and paleoclimate data and revisit the local, long-term variability mismatch (Laepple & Huybers, 2014a; Rehfeld et al., 2018; Ellerhoff & Rehfeld, 2021) using variance ratios. Figure 4 shows the model-data mismatch as variance ratios. The variance obtained from proxies is increasingly larger on longer timescales compared to that from simulated time series.

There is no major difference in the variance ratios between unforced and naturally forced runs on short timescales (2-5 and 5-50 years) (Fig. 3 (a) and (b)). This can be explained by internal processes dominating simulated local variability at these scales. The PI simulation slightly overestimate interannual variability in the mid and high latitudes compared to sea surface temperature observations of the last century.

Beyond periods of 50 years (Fig. 3 (c)-(e)), the simulated local variance is consistently smaller than proxy-based reconstructions. Inclusion of natural forcing in simulations decreases the mismatch for the majority of proxy sample sites. On periods of 50 to 200 years, the ratio bias is decreased by a factor (local mean improvement, Appendix A) of f=1.38 (1.12, 1.71, 90% confidence interval). The local mean improvement increases towards multicentennial scales, reducing the discrepancy. On periods of 200 to 500 years, the mismatch is reduced by a factor of 2.22 (1.75, 2.81) and 1.54 (1.27, 1.87) for the Last Glacial and Pre-Industrial, respectively. Although the inclusion of natural forcing is not sufficient to achieve consistency between modeled and proxy variance, it significantly reduces the mismatch.

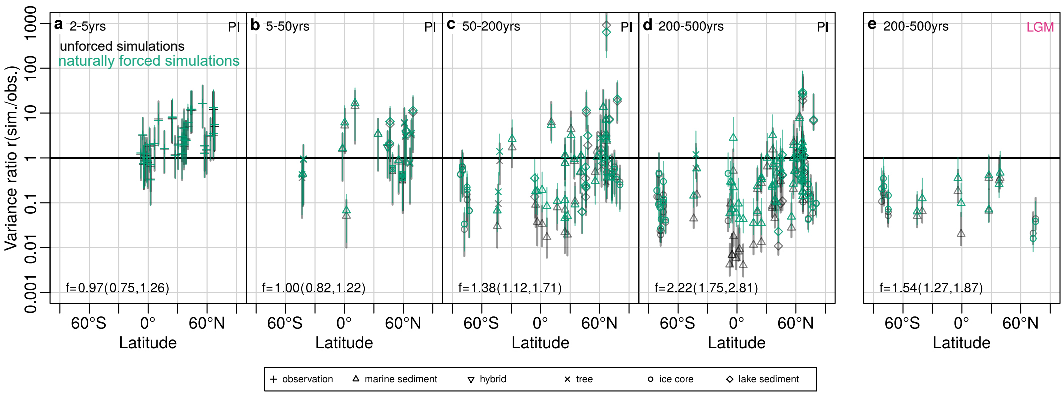

Figure 4. Ratio r(sim./obs.) of simulated to observed variance over latitude for unforced (black) and naturally forced (green) HadCM3 simulations. Model data is bilinearly interpolated to the location of the observation. We show the ratio of simulated PI temperature to observations for periods of 2-5 years (**a**), and to proxies spanning the last 8000 years on interannual to decadal (**b**), multidecadal (**c**), and multicentennial (**d**) timescales. Symbols indicate the variance ratio and vertical lines their 90% confidence interval. Panel **e** is the same as **d** for proxies spanning the last 19000 to 27000 years. The local mean improvement f of the variance ratio is given in the lower left of each panel, with confidence intervals in parentheses (Text Appendix A).

4 Discussion

We confirm that including natural forcing promotes temperature variability in model simulations across a range of timescales. In contrast to some experiments in the literature, we find that the modeled response of global mean surface temperature does not strongly depend on the mean climate (Fig. 1 and 3). Locally, weak state-dependent effects occur (Fig. 2 and 3). Considering natural forcing significantly increases global mean temperature variability and reduces the model-data mismatch on local temperature variability, in particular on multidecadal and multicentennial scales (Fig. 4).

Previous studies suggested state-dependent effects of volcanic forcing on global and hemispheric climate (Berdahl & Robock, 2013; Muthers et al., 2015; Swingedouw et al., 2017; Zanchettin et al., 2016). These results were obtained using ensembles of large volcanic eruptions. The dependency in these has been primarily linked to nonlinear processes, sensitive to the initial state (Zanchettin et al., 2013). We argue that the response to individual volcanic eruptions may well depend on the climate state. However, globally averaged effects from changes in response mechanisms are small when considering more realistic forcing scenarios. A linear relation between GMST and external forcing has been found at various timescales (Geoffroy et al., 2013; MacMynowski et al., 2011;

Fredriksen & Rypdal, 2017). In our ensemble, the GMST response to the large-magnitude 1257 Samalas eruption shows no difference between LGM* and PI* (Figure S8 (a)). Global precipitation and sea ice concentration is only slightly enhanced in the LGM* (Figure S8 (b) and (c)). The mean climate also predominately determines the AMOC variability (Figure S9), which is smaller in the Last Glacial on multidecadal and multicentennial scales than in the PI (Jackson & Vellinga, 2013). However, under Last Glacial conditions, the AMOC strength and correlation length is increased by natural forcing (Figure S9). While the potential mechanisms of the intensification are still debated (Iwi et al., 2012; Mignot et al., 2011), they could lead to state-dependent modifications of long-term regional variability through natural forcing.

The question of state-dependent local variability has long motivated studies of past (Ditlevsen et al., 1996; Shao & Ditlevsen, 2016; Rehfeld et al., 2018) and future (Huntingford et al., 2013; Rehfeld et al., 2020; Olonscheck et al., 2021) climate. Our results reveal a decrease in mean local variability with warming (Fig. 3 (a)). Decreasing sea ice dynamics and a smaller meridional temperature gradient are suggested as major causes (Berdahl & Robock, 2013; Bethke et al., 2017; Bathiany et al., 2018; Olonscheck et al., 2021; Rehfeld et al., 2018; Brown et al., 2017). In line with these studies, we find a clear zonal pattern, with greater reduction of variability in the mid and high latitudes (Fig. 3 (b) and (c)). This is corroborated by the small discrepancy between short-term variability from observations and simulations in the mid and high latitudes (Fig. 4(a)). In contrast to our PI simulations, the sea surface temperature observations are affected by the recent global warming trend and sea ice retreat, potentially leading to the observed decrease in local, high-latitude variability.

Consistent across our experiments, we find regions with varying sea ice extent, primarily the Southern Oceans and Barents Sea, to be most affected by the effects of natural forcing. This is further supported by mean standardized anomalies of precipitation, sea level pressure, and wind speed over the North American ice sheet, the North Atlantic Ocean, Antarctica, and the Southern Oceans (Figure S3). Moreover, the variability of global sea ice concentration is higher in forced compared to unforced scenarios (Figure S5). A comparison to simulations with the two-dimensional energy balance model (TransEBM (Ziegler & Rehfeld, 2021)) (Figure S6) adds support to the role of sea ice in forced temperature variability. As TransEBM is a fairly linear model with no atmospheric and oceanic dynamics, it can be used to differentiate the contribution from deterministic forcing and sea ice to the variance. We modified TransEBM to incorporate sea ice changes following the HadCM3 output. Forming the ratio of the local mean TransEBM and HadCM3 (Figure S7) reveals a strong sea ice contribution to interannual variability in line with Fig. 3 (a). The contribution remains significant on decadal and longer timescales, promoting sea ice variations as a key mechanism of local, long-term variability.

Our results provide crucial insights into the discrepancy between modeled and reconstructed local, long-term variability (Laepple & Huybers, 2014a; Ellerhoff & Rehfeld, 2021). While internal variability dominates the local temperature variance on annual to decadal scales (Goosse et al., 2005), we demonstrate contributions from natural forcing beyond decadal timescales (Fig. 3). This is supported by increased scaling coefficients (Figure S4) of forced temperatures on periods of 50 to 500 years, and implies an increase in variance on longer timescales. Including natural forcing in model simulations reveals a better model-data agreement of local variability on multidecadal and multicentennial scales (Fig. 4). This is perhaps surprising given that the forcing has no centennial scale variability (Ellerhoff & Rehfeld, 2021). There is no change in agreement from interannual to decadal timescales, implying that the gain from forcing on local temperatures is small on these short timescales. This suggests that not only the integrated response to strong (Timmreck, 2012) but also to weak natural forcing contributes to long-term variability. Time-varying forcing appears thus beneficial for reliable simulations of global mean (Fig. 3) and local, long-term variability. Consistent with previous arguments (Bethke et al., 2017), our results challenge the common usage of external forcing that is either constant or shows no time-varying changes besides a global trend (O'Neill et al., 2016).

We may miss feedback processes in our model simulations, that are relevant for local climate variability. This could explain the underestimation of local variability compared to proxy data (Fig. 4(a)). Sea ice dynamics, stratospheric and cloud-related feedbacks are key nonlinear mechanisms that can alter the response to volcanic forcing in a warmer climate (Hopcroft et al., 2018; Fasullo et al., 2017; Aubry et al., 2021). Projections for tropical volcanism showed enhanced radiative forcing from strong eruptions and a damping of the response to moderate eruptions (Aubry et al., 2021). The cloud-related feedback, likely to be underestimated in HadCM3, is generally weaker than that from sea ice, but may be enhanced in warmer climates (Hopcroft et al., 2018). While our results suggest that sea ice indeed is critical, it also highlights the role of the cryosphere response in setting climate variability. Future work could therefore examine the response in simulations with models that show a higher equilibrium climate sensitivity (Wu et al., 2019; Tatebe et al., 2019; Voldoire et al., 2019; Gettelman et al., 2019) and show more sensitive sea ice changes (Guarino et al., 2020). The absence of sea ice and changes in vegetation cover may significantly alter the response in extreme warming scenarios. In our long transient simulations, only one possible realization of the forcing history was considered. Future studies could therefore apply probabilistic representations (Bethke et al., 2017) to replicate results in larger ensembles (Zanchettin et al., 2016). This will also aid understanding of the state-dependent response of multidecadal modes to natural forcing (Swingedouw et al., 2017).

5 Conclusion

Presenting the first millennial-length, naturally forced simulation for the LGM, we investigated state-dependent effects of volcanic and solar forcing on global and local climate variability. The modeled global temperature response shows no dependency on the mean climate. Weak local differences resulted primarily from sea ice dynamics, providing a key mechanism of long-term variability. Including natural forcing in climate model simulations improved the agreement between modeled and observed variability and, thus, calls into question constant volcanic forcing in climate model simulations used for projections and model-data comparison. The robust temperature response suggests that findings on the ability of models to simulate past variability should translate to future climates; and can help constrain forced variability across spatial and temporal scales.

Appendix A Variance Ratio Improvement

We quantify the change in variance ratio r from unforced and naturally forced simulations to proxy records using the logarithmic measure $l(x) = |\log_{10}(x)|$. Let $r_i^{(*)} = \mathrm{var}(S_i^{(*)})\,/\mathrm{var}(S_i')$ be the variance ratio obtained from the simulated $S_i^{(*)}$ and proxy spectrum S_i' at the site i, with $(^*)$ denoting the climate state. The distance $l_i = l(r_i^*) - l(r_i)$ denotes the change of the variance ratio bias between the forced and unforced simulation. For a set of N sites, we quantify the mean change from $\Delta l = \frac{1}{N}\sum_i^N l_i w_i$ with local area weights w_i derived from the HadCM3 grid where $\sum_i^N w_i = 1$. We convert the logarithmic distance to the factor $f = 10^{\Delta l}$, called the variance ratio improvement. Similarly, we estimate the confidence ranges using area-weighted mean of the error propagation

$$\delta l_i = \sqrt{\left(\frac{\delta r_i^*}{r_i^* \ln(10)}\right)^2 + \left(\frac{\delta r_i}{r_i \ln(10)}\right)^2}\,. \tag{A1}$$

We ensure a conservative coverage of the confidence intervals by using the upper limit on $\delta r_i^{(*)}$ from the F-distributed uncertainties of the variance ratio estimate.

Open Research

The presented model simulations are available at Zenodo via 10.5281/zenodo.6074747 with CC-BY-SA 4.0 license. They were carried out using version 3 of the Hadley Center Coupled Model, HadCM3, are described in Valdes et al. (2017) and Tindall et al. (2009). The HadCM3 simulation ensemble was created using the Archer UK National Supercomputing Services. Paleoclimate and observation datasets for this research are included in Rehfeld et al. (2018); PAGES2k-Consortium (2017) and Rayner et al. (2003). Supplemental analysis was conducted using the two-dimensional TransEBM model as described by Ziegler and Rehfeld (2021) which is based on Zhuang et al. (2017). Code and data to reproduce all figures is available at `https://github.com/paleovar/StateDependency`, this will be deposited on Zenodo after peer review.

Acknowledgments

This research used the Archer UK National Supercomputing Services. It benefited from discussions within the CVAS working group, a working group of the Past Global Changes (PAGES) project. We thank M. Casado, T. Laepple and A. Schurer for discussion, and C. Wirths for setting up volcanic forcing over latitude intervals in TransEBM. Research has been funded by the PalMod project (`www.palmod.de`, subproject no. 01LP1926C), by the Deutsche Forschungsgemeinschaft (DFG, German Research Foundation) – project no. 395588486 and no. 316076679, and by the Heinrich-Böll-Stiftung.

References

Ambrose, S. H. (1998). Late pleistocene human population bottlenecks, volcanic winter, and differentiation of modern humans. *Journal of human evolution*, *34*(6), 623–651.

Armstrong, E., Izumi, K., & Valdes, P. (2022). No Title. *Climate Dynamics*. Retrieved from `https://doi.org/10.21203/rs.3.rs-715149/v1` doi: 10.21203/rs.3.rs-715149/v1

Aubry, T. J., Staunton-Sykes, J., Marshall, L. R., Haywood, J., Abraham, N. L., & Schmidt, A. (2021). Climate change modulates the stratospheric volcanic sulfate aerosol lifecycle and radiative forcing from tropical eruptions. *Nature Communications*, *12*. doi: 10.1038/s41467-021-24943-7

Baldini, J. U., Brown, R. J., & McElwaine, J. N. (2015). Was millennial scale climate change during the Last Glacial triggered by explosive volcanism? *Scientific Reports*, *5*, 1–9. doi: 10.1038/srep17442

Bathiany, S., Dakos, V., Scheffer, M., & Lenton, T. M. (2018). Climate models predict increasing temperature variability in poor countries. *Science Advances*, *4*(5), eaar5809. doi: 10.1126/sciadv.aar5809

Berdahl, M., & Robock, A. (2013). Northern hemispheric cryosphere response to volcanic eruptions in the paleoclimate modeling intercomparison project 3 last millennium simulations. *Journal of Geophysical Research Atmospheres*, *118*, 12,359-12,370. doi: 10.1002/2013JD019914

Berger, A. L. (1978). Long-term variations of daily insolation and Quaternary climatic changes. *Journal of Atmospheric Sciences*, *35*(12), 2361–2367. doi: 10.1175/1520-0469(1978)035⟨2362:ltvodi⟩2.0.co;2

Bethke, I., Outten, S., Otterå, O. H., Hawkins, E., Wagner, S., Sigl, M., & Thorne, P. (2017). Potential volcanic impacts on future climate variability. *Nature Climate Change*. doi: 10.1038/nclimate3394

Bindoff, N. L., Stott, P. A., AchutaRao, K. M., Allen, M. R., Gillett, N., Gutzler, D., … Zhang, X. (2013). Detection and attribution of climate change: From global to regional. In T. F. Stocker et al. (Eds.), *Climate change 2013: The physical science basis. contribution of working group i to the fifth assessment report of the intergovernmental panel on climate* *change* (pp. 867–952). Cambridge, UK: Cambridge University Press. doi: 10.1017/CBO9781107415324.022

Braconnot, P., Harrison, S. P., Kageyama, M., Bartlein, P. J., Masson-Delmotte, V., Abe-Ouchi, A., . . . Zhao, Y. (2012). Evaluation of climate models using palaeoclimatic data. *Nature Climate Change*, *2*, 417-424. doi: 10.1038/nclimate1456

Brad Adams, J., Mann, M. E., & Ammann, C. M. (2003). Proxy evidence for an El Niño-like response to volcanic forcing. *Nature*, *426*(6964), 274–278. doi: 10.1038/nature02101

Brown, P. T., Ming, Y., Li, W., & Hill, S. A. (2017). Change in the magnitude and mechanisms of global temperature variability with warming. *Nature Climate Change*. doi: 10.1038/nclimate3381

Bühler, J. C., Roesch, C., Kirschner, M., Sime, L., Holloway, M., & Rehfeld, K. (2021). Comparison of the oxygen isotope signatures in speleothem records and ihadcm3 model simulations for the last millennium. *Climate of The Past*, 1-30. doi: 10.5194/cp-2020-121

Casado, M., Münch, T., & Laepple, T. (2020). Climatic information archived in ice cores: impact of intermittency and diffusion on the recorded isotopic signal in antarctica. *Climate of the Past*, *16*, 1581-1598. doi: 10.5194/cp-16-1581-2020

Collins, M., Tett, S., & Cooper, C. (2001). The internal climate variability of hadcm3, a version of the hadley centre coupled model without flux adjustments. *Climate Dynamics*, *17*(1), 61–81.

Cox, P. M. (2001). Description of the" triffid" dynamic global vegetation model. *Hadley Centre Technical Note*.

Crowley, T. J. (2000). Causes of climate change over the past 1000 years. *Science*. doi: 10.1126/science.289.5477.270

Crowley, T. J., & Unterman, M. B. (2013). Technical details concerning development of a 1200 yr proxy index for global volcanism. *Earth System Science Data*, *5*, 187-197. doi: 10.5194/essd-5-187-2013

Danabasoglu, G., Yeager, S. G., Kwon, Y.-O., Tribbia, J. J., Phillips, A. S., & Hurrell, J. W. (2012). Variability of the atlantic meridional overturning circulation in ccsm4. *Journal of climate*, *25*(15), 5153–5172.

Davies, N., & Chatfield, C. (1990). The analysis of time series: An introduction. *The Mathematical Gazette*. doi: 10.2307/3619403

Ditlevsen, P. D., Svensmark, H., & Johnsen, S. (1996). Contrasting atmospheric and climate dynamics of the last-glacial and holocene periods. *Nature*, *379*. doi: 10.1038/379810a0

Ellerhoff, B., & Rehfeld, K. (2021, Dec). Probing the timescale dependency of local and global variations in surface air temperature from climate simulations and reconstructions of the last millennia. *Phys. Rev. E*, *104*, 064136. doi: 10.1103/PhysRevE.104.064136

Fasullo, J. T., Tomas, R., Stevenson, S., Otto-Bliesner, B., Brady, E., & Wahl, E. (2017). The amplifying influence of increased ocean stratification on a future year without a summer. *Nature Communications*, *8*. doi: 10.1038/s41467-017-01302-z

Flato, G., Marotzke, J., Abiodun, B., Braconnot, P., Chou, S., Collins, W., . . . Rummukainen, M. (2014). Evaluation of climate models. In T. Stocker et al. (Eds.), (Vol. 9781107057999, p. 741-866). Cambridge University Press. doi: 10.1017/CBO9781107415324.020

Forster, P., Storelvmo, T., Armour, K., Collins, W., Dufresne, J. L., Frame, D., . . . Zhang, H. (2021). The Earth's Energy Budget, Climate Feedbacks, And Climate Sensitivity. In V. Masson-Delmotte et al. (Eds.), *Climate change 2021: The physical science basis. contribution of working group i to the sixth assessment report of the intergovernmental panel on climate change* (chap. 7). Cambridge: Cambridge University Press.

Frankcombe, L. M., England, M. H., Mann, M. E., & Steinman, B. A. (2015). Separating internal variability from the externally forced climate response. *Journal of Climate*, *28*(20), 8184–8202. doi: 10.1175/JCLI-D-15-0069.1

Franzke, C. L., Barbosa, S., Blender, R., Fredriksen, H., Laepple, T., Lambert, F., ... Yuan, N. (2020). The structure of climate variability across scales. *Reviews of Geophysics*. doi: 10.1029/2019RG000657

Fredriksen, H. B., & Rypdal, K. (2016). Spectral characteristics of instrumental and climate model surface temperatures. *Journal of Climate*, *29*, 1253-1268. doi: 10.1175/JCLI-D-15-0457.1

Fredriksen, H. B., & Rypdal, M. (2017). Long-range persistence in global surface temperatures explained by linear multibox energy balance models. *Journal of Climate*, *30*, 7157-7168. doi: 10.1175/JCLI-D-16-0877.1

Geoffroy, O., Saint-martin, D., Olivié, D. J., Voldoire, A., Bellon, G., & Tytéca, S. (2013). Transient climate response in a two-layer energy-balance model. Part I: Analytical solution and parameter calibration using CMIP5 AOGCM experiments. *Journal of Climate*, *26*(6), 1841–1857. doi: 10.1175/JCLI-D-12-00195.1

Gettelman, A., Hannay, C., Bacmeister, J. T., Neale, R. B., Pendergrass, A., Danabasoglu, G., ... others (2019). High climate sensitivity in the community earth system model version 2 (cesm2). *Geophysical Research Letters*, *46*(14), 8329–8337.

Goosse, H., Renssen, H., Timmermann, A., & Bradley, R. S. (2005). Internal and forced climate variability during the last millennium: A model-data comparison using ensemble simulations. *Quaternary Science Reviews*, *24*, 1345-1360. doi: 10.1016/j.quascirev.2004.12.009

Gordon, C., Cooper, C., Senior, C. A., Banks, H., Gregory, J. M., Johns, T. C., ... Wood, R. A. (2000, 7). The simulation of sst, sea ice extents and ocean heat transports in a version of the hadley centre coupled model without flux adjustments. *Climate Dynamics*, *16*, 147-168. doi: 10.1007/s003820050010

Guarino, M.-V., Sime, L. C., Schröeder, D., Malmierca-Vallet, I., Rosenblum, E., Ringer, M., ... others (2020). Sea-ice-free arctic during the last interglacial supports fast future loss. *Nature Climate Change*, *10*(10), 928–932.

Halloran, P. R., Hall, I. R., Menary, M., Reynolds, D. J., Scourse, J. D., Screen, J. A., ... Garry, F. (2020). Natural drivers of multidecadal Arctic sea ice variability over the last millennium. *Scientific Reports*, *10*(1), 1–9. doi: 10.1038/s41598-020-57472-2

Hasselmann, K. (1997). Multi-pattern fingerprint method for detection and attribution of climate change. *Climate Dynamics*, *13*(9), 601–611. Retrieved from `https://doi.org/10.1007/s003820050185` doi: 10.1007/s003820050185

Haustein, K., Otto, F. E., Venema, V., Jacobs, P., Cowtan, K., Hausfather, Z., ... Schurer, A. P. (2019). A limited role for unforced internal variability in twentieth-century warming. *Journal of Climate*, *32*(16), 4893–4917. doi: 10.1175/JCLI-D-18-0555.1

Holmes, C. R., Woollings, T., Hawkins, E., & de Vries, H. (2016). Robust future changes in temperature variability under greenhouse gas forcing and the relationship with thermal advection. *Journal of Climate*, *29*(6), 2221–2236. doi: 10.1175/JCLI-D-14-00735.1

Hopcroft, P. O., Kandlbauer, J., Valdes, P. J., & Sparks, R. S. J. (2018). Reduced cooling following future volcanic eruptions. *Climate Dynamics*, *51*, 1449-1463. doi: 10.1007/s00382-017-3964-7

Huntingford, C., Jones, P. D., Livina, V. N., Lenton, T. M., & Cox, P. M. (2013). No increase in global temperature variability despite changing regional patterns. *Nature*. doi: 10.1038/nature12310

Huybers, P., & Curry, W. (2006). Links between annual, milankovitch and continuum temperature variability. *Nature*, *441*, 329-332. doi: 10.1038/nature04745

Iwi, A. M., Hermanson, L., Haines, K., & Sutton, R. T. (2012). Mechanisms linking volcanic aerosols to the atlantic meridional overturning circulation. *Journal of Climate*, *25*, 3039-3051. doi: 10.1175/2011JCLI4067.1

Jackson, L., & Vellinga, M. (2013). Multidecadal to centennial variability of the amoc: Hadcm3 and a perturbed physics ensemble. *Journal of climate*, *26*(7), 2390–2407.

Kageyama, M., Braconnot, P., Harrison, S. P., Haywood, A. M., Jungclaus, J. H., Otto-Bliesner, B. L., ... Zhou, T. (2018). The pmip4 contribution to cmip6 - part 1: Overview and over-arching analysis plan. *Geoscientific Model Development*, *11*. doi: 10.5194/gmd-11-1033-2018

Katz, R. W., & Brown, B. G. (1992). Extreme events in a changing climate: Variability is more important than averages. *Climatic Change*, 289-302.

Laepple, T., & Huybers, P. (2014a). Global and regional variability in marine surface temperatures. *Geophysical Research Letters*, *41*, 2528-2534. doi: 10.1002/2014GL059345

Laepple, T., & Huybers, P. (2014b). Ocean surface temperature variability: Large model–data differences at decadal and longer periods. *Proceedings of the National Academy of Sciences*, *111*, 16682-16687. doi: 10.1073/pnas.1412077111

Laepple, T., Münch, T., Casado, M., Hoerhold, M., Landais, A., & Kipfstuhl, S. (2018). On the similarity and apparent cycles of isotopic variations in east antarctic snow pits. *Cryosphere*. doi: 10.5194/tc-12-169-2018

Lovejoy, S., & Varotsos, C. (2016). Scaling regimes and linear/nonlinear responses of last millennium climate to volcanic and solar forcings. *Earth System Dynamics*, *7*, 133-150. doi: 10.5194/esd-7-133-2016

MacMynowski, D. G., Shin, H.-J., & Caldeira, K. (2011). The frequency response of temperature and precipitation in a climate model. *Geophysical Research Letters*, *38*, n/a-n/a. doi: 10.1029/2011GL048623

Mann, M. E., Steinman, B. A., Brouillette, D. J., Fernandez, A., & Miller, S. K. (2022). On The Estimation of Internal Climate Variability During the Preindustrial Past Millennium. *Geophysical Research Letters*, *n/a*(n/a), e2021GL096596. Retrieved from `https://agupubs.onlinelibrary.wiley.com/doi/abs/10.1029/2021GL096596` doi: https://doi.org/10.1029/2021GL096596

Marcott, S. A., Shakun, J. D., Clark, P. U., & Mix, A. C. (2013). A Reconstruction of Regional and Global Temperature for the Past 11,300 Years. *Science*, *339*(6124), 1198–1201. Retrieved from `https://www.science.org/doi/abs/10.1126/science.1228026` doi: 10.1126/science.1228026

Mignot, J., Khodri, M., Frankignoul, C., & Servonnat, J. (2011). Volcanic impact on the atlantic ocean over the last millennium. *Climate of the Past*, *7*(4), 1439–1455.

Muthers, S., Arfeuille, F., Raible, C. C., & Rozanov, E. (2015). The impacts of volcanic aerosol on stratospheric ozone and the northern hemisphere polar vortex: Separating radiative-dynamical changes from direct effects due to enhanced aerosol heterogeneous chemistry. *Atmospheric Chemistry and Physics*, *15*, 11461-11476. doi: 10.5194/acp-15-11461-2015

Nilsen, T., Rypdal, K., & Fredriksen, H. B. (2016). Are there multiple scaling regimes in holocene temperature records? *Earth System Dynamics*, *7*, 419-439. doi: 10.5194/esd-7-419-2016

Olonscheck, D., Schurer, A. P., Lücke, L., & Hegerl, G. C. (2021). Large-scale emergence of regional changes in year-to-year temperature variability by the end of the 21st century. *Nature Communications*, *12*(1), 7237. doi: 10.1038/s41467-021-27515-x

O'Neill, B. C., Tebaldi, C., Vuuren, D. P. V., Eyring, V., Friedlingstein, P., Hurtt, G., ... Sanderson, B. M. (2016). The scenario model intercomparison project (scenariomip) for cmip6. *Geoscientific Model Development*, *9*. doi:

10.5194/gmd-9-3461-2016
PAGES2k-Consortium. (2017). A global multiproxy database for temperature reconstructions of the common era. *Scientific Data*, *4*, 1-33. doi: DOI:10.1038/sdata.2017.88

Pendergrass, A. G., Knutti, R., Lehner, F., Deser, C., & Sanderson, B. M. (2017). Precipitation variability increases in a warmer climate. *Scientific Reports*, *7*. doi: 10.1038/s41598-017-17966-y

Percival, D. B., & Walden, A. T. (1993). *Spectral analysis for physical applications: Multitaper and conventional univariate techniques.* Cambridge University Press. doi: 10.1017/CBO9780511622762

Pope, V., Gallani, M., Rowntree, P., & Stratton, R. (2000). The impact of new physical parametrizations in the hadley centre climate model: Hadam3. *Climate dynamics*, *16*(2-3), 123–146.

Rayner, N. A., Parker, D. E., Horton, E. B., Folland, C. K., Alexander, L. V., Rowell, D. P., . . . Kaplan, A. (2003). Global analyses of sea surface temperature, sea ice, and night marine air temperature since the late nineteenth century. *Journal of Geophysical Research: Atmospheres*, *108*(D14). doi: https://doi.org/10.1029/2002JD002670

Rehfeld, K., Hébert, R., Lora, J., Lofverstrom, M., & Brierley, C. (2020). Variability of surface climate in simulations of past and future. *Earth System Dynamics*, 1-30. doi: 10.5194/esd-2019-92

Rehfeld, K., Münch, T., Ho, S. L., & Laepple, T. (2018). Global patterns of declining temperature variability from the last glacial maximum to the holocene. *Nature*, *554*, 356-359. doi: 10.1038/nature25454

Reichler, T., & Kim, J. (2008). How well do coupled models simulate today's climate? *Bulletin of the American Meteorological Society*, *89*(3), 303 - 312. doi: 10.1175/BAMS-89-3-303

Robock, A. (2000, 5). Volcanic eruptions and climate. *Reviews of Geophysics*, *38*, 191-219. doi: 10.1029/1998RG000054

Schmidt, G. A., Jungclaus, J. H., Ammann, C. M., Bard, E., Braconnot, P., Crowley, T. J., . . . Vieira, L. E. A. (2012). Climate forcing reconstructions for use in pmip simulations of the last millennium (v1.1). *Geoscientific Model Development*, *5*, 185-191. doi: 10.5194/gmd-5-185-2012

Schurer, A. P., Hegerl, G. C., Mann, M. E., Tett, S. F. B., & Phipps, S. J. (2013, sep). Separating Forced from Chaotic Climate Variability over the Past Millennium. *Journal of Climate*, *26*(18), 6954–6973. doi: 10.1175/JCLI-D-12-00826.1

Sear, C. B., Kelly, P. M., Jones, P. D., & Goodess, C. M. (1987). Global surface-temperature responses to major volcanic eruptions. *Nature*, *330*(6146), 365–367. Retrieved from `https://doi.org/10.1038/330365a0` doi: 10.1038/330365a0

Shao, Z. . G., & Ditlevsen, P. D. (2016). Contrasting scaling properties of interglacial and glacial climates. *Nat. Commun.*, *7*. doi: 10.1038/ncomms10951

Singarayer, J. S., & Valdes, P. J. (2010). High-latitude climate sensitivity to ice-sheet forcing over the last 120 kyr. *Quaternary Science Reviews*, *29*, 43-55. doi: 10.1016/j.quascirev.2009.10.011

Sippel, S., Meinshausen, N., Fischer, E. M., Székely, E., & Knutti, R. (2020). Climate change now detectable from any single day of weather at global scale. *Nature Climate Change*, *10*(1), 35–41. Retrieved from `https://doi.org/10.1038/s41558-019-0666-7` doi: 10.1038/s41558-019-0666-7

Steinhilber, F., Beer, J., & Fröhlich, C. (2009). Total solar irradiance during the holocene. *Geophysical Research Letters*, *36*, 1-5. doi: 10.1029/2009GL040142

Stott, P. A., Tett, S. F., Jones, G. S., Allen, M., Mitchell, J., & Jenkins, G. (2000). External control of 20th century temperature by natural and anthropogenic forcings. *science*, *290*(5499), 2133–2137.

Svensson, A., Bigler, M., Blunier, T., Clausen, H. B., Dahl-Jensen, D., Fischer, H., ... Winstrup, M. (2013). Direct linking of greenland and antarctic ice cores at the toba eruption (74 ka bp). *Climate of the Past*, *9*(2), 749–766. Retrieved from `https://cp.copernicus.org/articles/9/749/2013/` doi: 10.5194/cp-9-749-2013

Swingedouw, D., Mignot, J., Ortega, P., Khodri, M., Menegoz, M., Cassou, C., & Hanquiez, V. (2017). Impact of explosive volcanic eruptions on the main climate variability modes. *Global and Planetary Change*, *150*, 24-45. doi: 10.1016/j.gloplacha.2017.01.006

Tatebe, H., Ogura, T., Nitta, T., Komuro, Y., Ogochi, K., Takemura, T., ... others (2019). Description and basic evaluation of simulated mean state, internal variability, and climate sensitivity in miroc6. *Geoscientific Model Development*, *12*(7), 2727–2765.

Timmreck, C. (2012). Modeling the climatic effects of large explosive volcanic eruptions. *Wiley Interdisciplinary Reviews: Climate Change*, *3*. doi: 10.1002/wcc.192

Timmreck, C., Graf, H.-F., Lorenz, S. J., Niemeier, U., Zanchettin, D., Matei, D., ... Crowley, T. J. (2010). Aerosol size confines climate response to volcanic super-eruptions. *Geophysical Research Letters*, *37*(24). doi: 10.1029/2010GL045464

Tindall, J. C., Valdes, P. J., & Sime, L. C. (2009). Stable water isotopes in hadcm3: Isotopic signature of el niño-southern oscillation and the tropical amount effect. *Journal of Geophysical Research: Atmospheres*, *114*, 1-12. doi: 10.1029/2008JD010825

Valdes, P. J., Armstrong, E., Badger, M. P. S., Bradshaw, C. D., Bragg, F., Crucifix, M., ... Williams, J. H. T. (2017). The bridge hadcm3 family of climate models: Hadcm3@bristol v1.0. *Geoscientific Model Development*, *10*(10), 3715–3743. Retrieved from `https://gmd.copernicus.org/articles/10/3715/2017/` doi: 10.5194/gmd-10-3715-2017

Voldoire, A., Saint-Martin, D., Sénési, S., Decharme, B., Alias, A., Chevallier, M., ... others (2019). Evaluation of cmip6 deck experiments with cnrm-cm6-1. *Journal of Advances in Modeling Earth Systems*, *11*(7), 2177–2213.

Wang, T., Miao, J., Wang, H., & Sun, J. (2021). Influence of Strong Tropical Volcanic Eruptions on Daily Temperature and Precipitation Extremes Across the Globe. *Journal of Meteorological Research*, *35*(3), 428–443. Retrieved from `https://doi.org/10.1007/s13351-021-0160-9` doi: 10.1007/s13351-021-0160-9

Wang, Y., Lean, J. L., & Jr., N. R. S. (2005). Modeling the sun's magnetic field and irradiance since 1713. *The Astrophysical Journal*, *625*, 522-538. doi: 10.1086/429689

Wu, T., Lu, Y., Fang, Y., Xin, X., Li, L., Li, W., ... others (2019). The beijing climate center climate system model (bcc-csm): the main progress from cmip5 to cmip6. *Geoscientific Model Development*, *12*(4), 1573–1600.

Zanchettin, D., Bothe, O., Graf, H. F., Lorenz, S. J., Luterbacher, J., Timmreck, C., & Jungclaus, J. H. (2013). Background conditions influence the decadal climate response to strong volcanic eruptions. *Journal of Geophysical Research Atmospheres*, *118*, 4090-4106. doi: 10.1002/jgrd.50229

Zanchettin, D., Khodri, M., Timmreck, C., Toohey, M., Schmidt, A., Gerber, E. P., ... Tummon, F. (2016). The model intercomparison project on the climatic response to volcanic forcing (volmip): Experimental design and forcing input data for cmip6. *Geoscientific Model Development*, *9*, 2701-2719. doi: 10.5194/gmd-9-2701-2016

Zhuang, K., North, G. R., & Stevens, M. J. (2017). A netcdf version of the two-dimensional energy balance model based on the full multigrid algorithm. *SoftwareX*, *6*, 198-202. doi: 10.1016/j.softx.2017.07.003

Ziegler, E., & Rehfeld, K. (2021). Transebm v. 1.0: Description, tuning, and validation of a transient model of the earth's energy balance in two dimensions. *Geoscientific Model Development*, *14*, 2843-2866. doi: 10.5194/gmd-14-2843-2021

Supporting Information for "State-dependent effects of natural forcing on global and regional climate variability"

Beatrice Ellerhoff[1,2,3], Moritz J. Kirschner[1], Elisa Ziegler[1,2,3], Max D. Holloway[4], Louise Sime[5], Kira Rehfeld[1,2,3]

[1]Institute of Environmental Physics, Heidelberg, Germany

[2]Department of Physics and Department of Geoscience, Tübingen University, Tübingen, Germany

[3]Geo- und Umweltforschungszentrum, Tübingen University, Tübingen, Germany

[4]Scottish Association for Marine Science, Oban, United Kingdom

[5]British Antarctic Survey, Cambridge, United Kingdom

Contents of this file

1. Figures S1 to S11
2. Tables S1 and S2

Additional Supporting Information (Files uploaded separately)

1. Captions for Datasets S1

Introduction This supporting material provides additional information on boundary conditions, surface climate, and spectral properties of the HadCM3 simulation. We show the power spectra of all simulated and reconstructed time series, used for variance ratio estimates. The separately uploaded dataset S1 contains detailed information about the considered paleoclimate records from Rehfeld, Münch, Ho, and Laepple (2018), Rayner et al. (2003), and the PAGES2k-Consortium (2017). We provide a supporting analysis on the contribution of sea ice dynamics to variability using the two-dimensional TransEBM model (Ziegler & Rehfeld, 2021).

Data Set S1. Key specification of proxy records used to estimate local temperature variance ratios. The records were collected from Rehfeld et al. (2018), Rayner et al. (2003) and the PAGES2k-Consortium (2017). The first six columns denote the reconstruction name, assigned ID, location (Latitude, Longitude, Elevation), archive type, and proxy used. The last column denotes the climate state ("LGM" or "PI") for which the proxy reconstruction was considered. Surface temperature observations were taken from the location closest to the proxy location and specified by "HadISST@...".

References

Berger, A. L. (1978). Long-term variations of daily insolation and Quaternary climatic changes. *Journal of Atmospheric Sciences*, *35*(12), 2361–2367. doi: 10.1175/1520-0469(1978)035⟨2362:ltvodi⟩2.0.co;2

Brad Adams, J., Mann, M. E., & Ammann, C. M. (2003). Proxy evidence for an El Niño-like response to volcanic forcing. *Nature*, *426*(6964), 274–278. doi: 10.1038/nature02101

Cox, P. M. (2001). Description of the" triffid" dynamic global vegetation model. *Hadley Centre Technical Note*.

Crowley, T. J., & Unterman, M. B. (2013). Technical details concerning development of a 1200 yr proxy index for global volcanism. *Earth System Science Data*, *5*, 187-197. doi: 10.5194/essd-5-187-2013

Danabasoglu, G., Yeager, S. G., Kwon, Y.-O., Tribbia, J. J., Phillips, A. S., & Hurrell, J. W. (2012). Variability of the atlantic meridional overturning circulation in ccsm4. *Journal of climate*, *25*(15), 5153–5172.

Fredriksen, H. B., & Rypdal, M. (2017). Long-range persistence in global surface temperatures explained by linear multibox energy balance models. *Journal of Climate*, *30*, 7157-7168. doi: 10.1175/JCLI-D-16-0877.1

Huybers, P., & Curry, W. (2006). Links between annual, milankovitch and continuum temperature variability. *Nature*, *441*, 329-332. doi: 10.1038/nature04745

Lovejoy, S., & Varotsos, C. (2016). Scaling regimes and linear/nonlinear responses of last millennium climate to volcanic and solar forcings. *Earth System Dynamics*, *7*, 133-150. doi: 10.5194/esd-7-133-2016

PAGES2k-Consortium. (2017). A global multiproxy database for temperature reconstructions of the common era. *Scientific Data*, *4*, 1-33. doi: DOI:10.1038/sdata.2017.88

Rayner, N. A., Parker, D. E., Horton, E. B., Folland, C. K., Alexander, L. V., Rowell, D. P., … Kaplan, A. (2003). Global analyses of sea surface temperature, sea ice, and night marine air temperature since the late nineteenth century. *Journal of Geophysical Research: Atmospheres*, *108*(D14). doi: https://doi.org/10.1029/2002JD002670

Rehfeld, K., Münch, T., Ho, S. L., & Laepple, T. (2018). Global patterns of declining temperature variability from the last glacial maximum to the holocene. *Nature*, *554*, 356-359. doi: 10.1038/nature25454

Schmidt, G. A., Jungclaus, J. H., Ammann, C. M., Bard, E., Braconnot, P., Crowley, T. J., ... Vieira, L. E. A. (2012). Climate forcing reconstructions for use in pmip simulations of the last millennium (v1.1). *Geoscientific Model Development*, *5*, 185-191. doi: 10.5194/gmd-5-185-2012

Sear, C. B., Kelly, P. M., Jones, P. D., & Goodess, C. M. (1987). Global surface-temperature responses to major volcanic eruptions. *Nature*, *330*(6146), 365–367. Retrieved from `https://doi.org/10.1038/330365a0` doi: 10.1038/330365a0

Singarayer, J. S., & Valdes, P. J. (2010). High-latitude climate sensitivity to ice-sheet forcing over the last 120 kyr. *Quaternary Science Reviews*, *29*, 43-55. doi: 10.1016/j.quascirev.2009.10.011

Steinhilber, F., Beer, J., & Fröhlich, C. (2009). Total solar irradiance during the holocene. *Geophysical Research Letters*, *36*, 1-5. doi: 10.1029/2009GL040142

Wang, Y., Lean, J. L., & Jr., N. R. S. (2005). Modeling the sun's magnetic field and irradiance since 1713. *The Astrophysical Journal*, *625*, 522-538. doi: 10.1086/429689

Zhuang, K., North, G. R., & Stevens, M. J. (2017). A netcdf version of the two-dimensional energy balance model based on the full multigrid algorithm. *SoftwareX*, *6*, 198-202. doi: 10.1016/j.softx.2017.07.003

Ziegler, E., & Rehfeld, K. (2021). Transebm v. 1.0: Description, tuning, and validation of a transient model of the earth's energy balance in two dimensions. *Geoscientific Model Development*, *14*, 2843-2866. doi: 10.5194/gmd-14-2843-2021

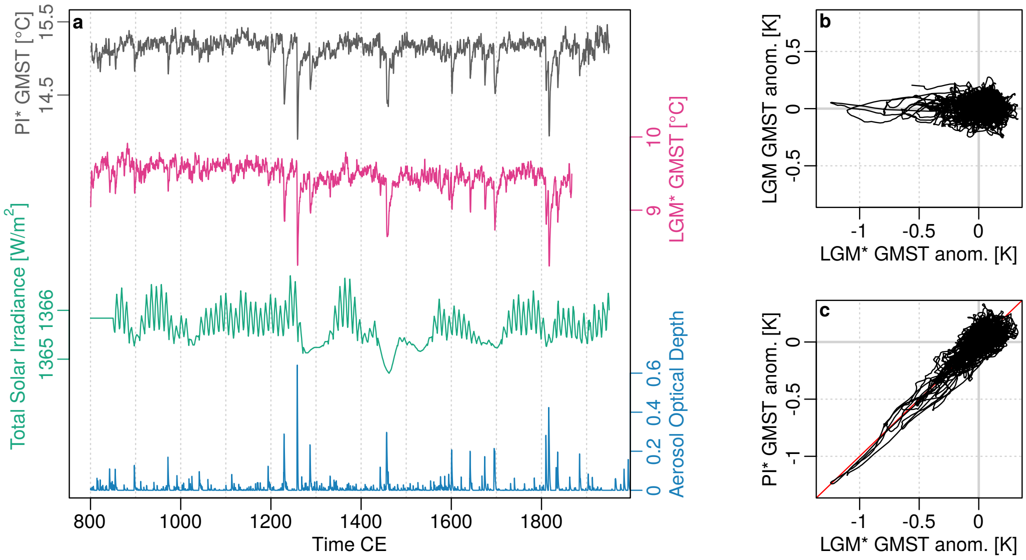

Figure S1. **a** Simulated PI* and LGM* global mean surface temperature (GMST) averaged over all runs in a state, total solar irradiance (Steinhilber et al., 2009), and aerosol optical depth (Crowley & Unterman, 2013). The solar forcing was kept constant the first 50 years due to missing reconstructions. **b** LGM over LGM* GMST anomalies from HadCM3 after linear detrending and subtracting the mean of the full time series. **c** As **b**, with PI* over LGM* GMST anomalies.

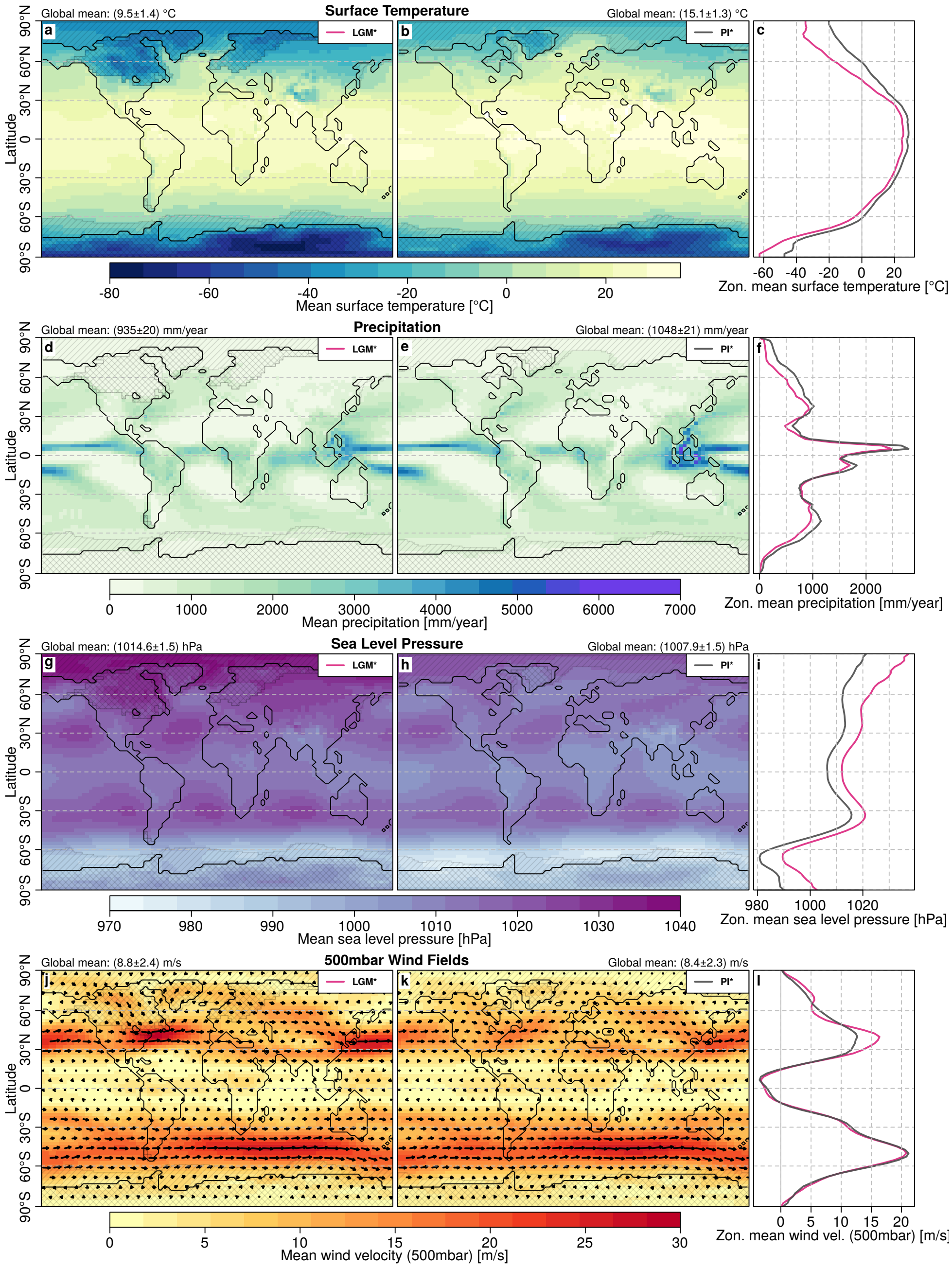

Figure S2. Surface temperature (**a-c**), precipitation rate (**d-f**), sea level pressure (**g-i**), and wind fields at 500mbar (**j-l**) as simulated by HadCM3 for the LGM* and PI*. Means over latitude intervals are displayed in the right-hand panels. Global mean values and their standard deviation are given above the maps.

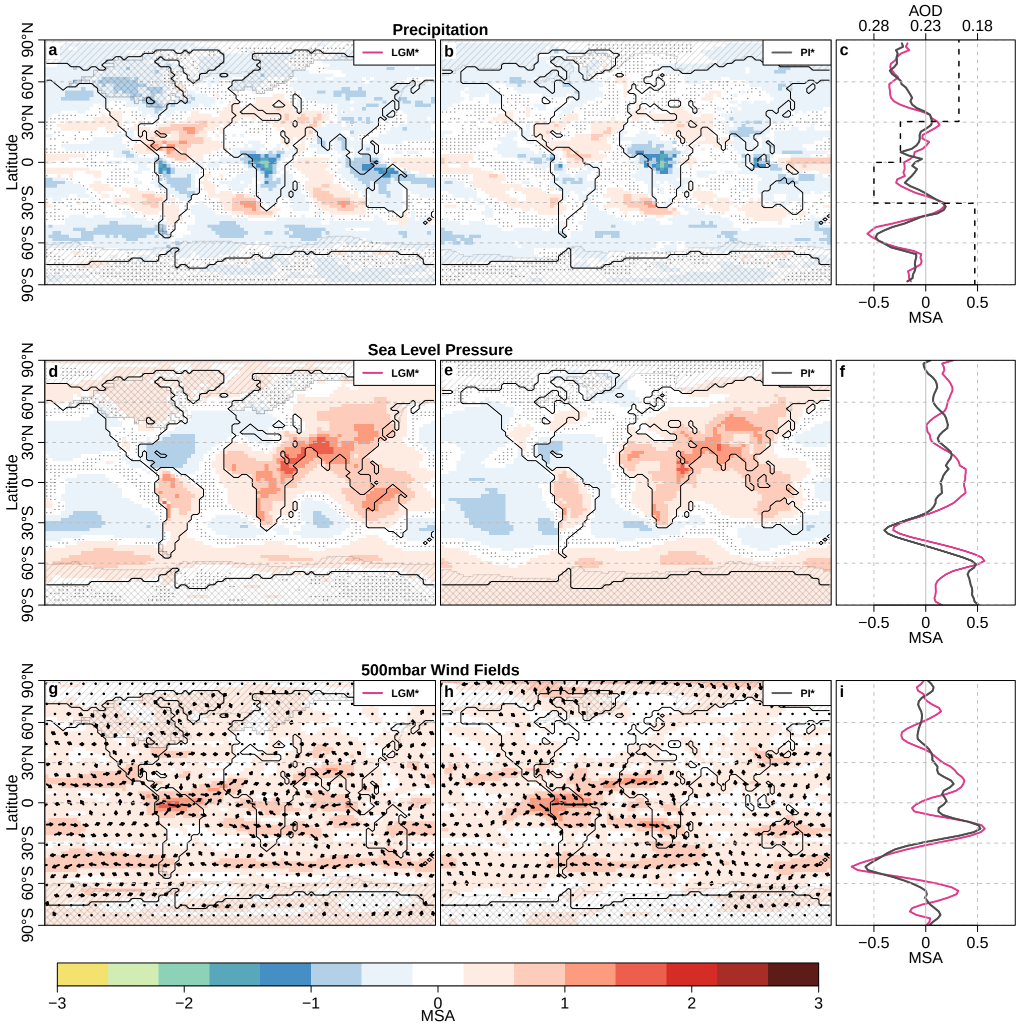

Figure S3. Mean standardized anomalies (MSA), as Figure 2 of the main manuscript, for precipitation rate (**a-c**), sea level pressure (**d-f**), and wind fields at 500mbar (**g-i**) from HadCM3. Dots indicate insignificant anomalies within the 99% quantile range of local variability. Grey shaded crosses and lines show land and sea ice, respectively. Mean anomalies over latitude intervals are displayed on the right-hand panels. The black dashed line shows the mean zonal Aerosol Optical Depth (AOD) imprint.

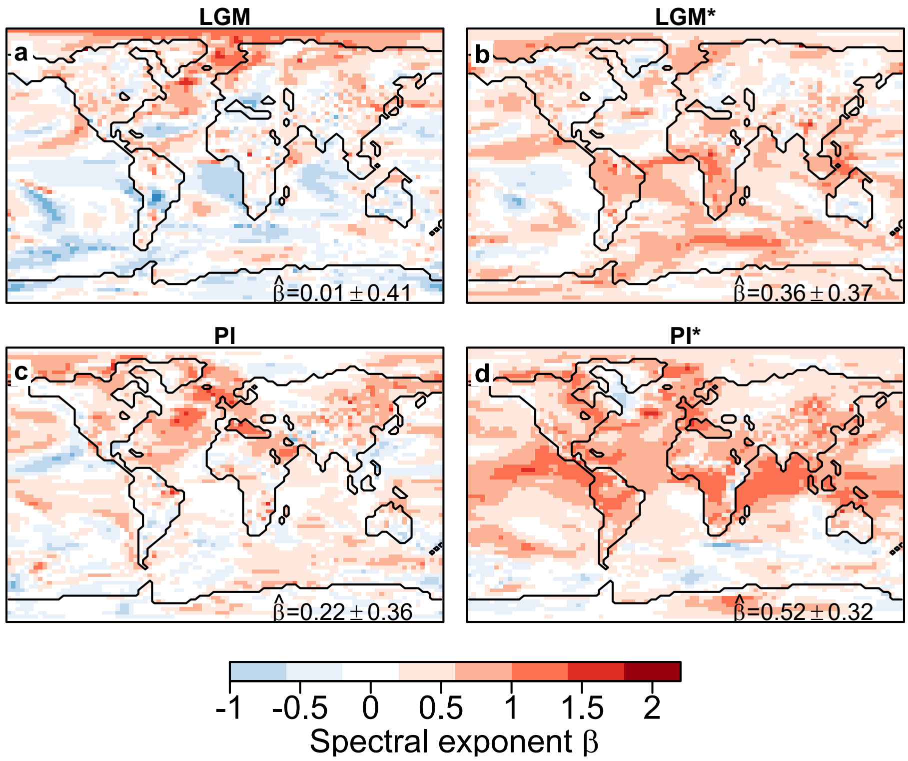

Figure S4. Scaling coefficient β of forced and unforced surface air temperature on the multidecadal-to-multicentennial scale (50-500yrs) as simulated by HadCM3 for the Last Glacial and Pre-Industrial. Surface air temperature variability was approximated by power-laws of the spectrum $S(\tau) \sim \tau^{\beta}$ with $50 \leq \tau \leq 500$ years and scaling coefficient β (Huybers & Curry, 2006; Fredriksen & Rypdal, 2017; Lovejoy & Varotsos, 2016). The area-weighted mean scaling coefficient is denoted by $\hat{\beta}$. Following Huybers and Curry (2006), we estimate β by linear regression after log-binning to prevent low-frequency biases.

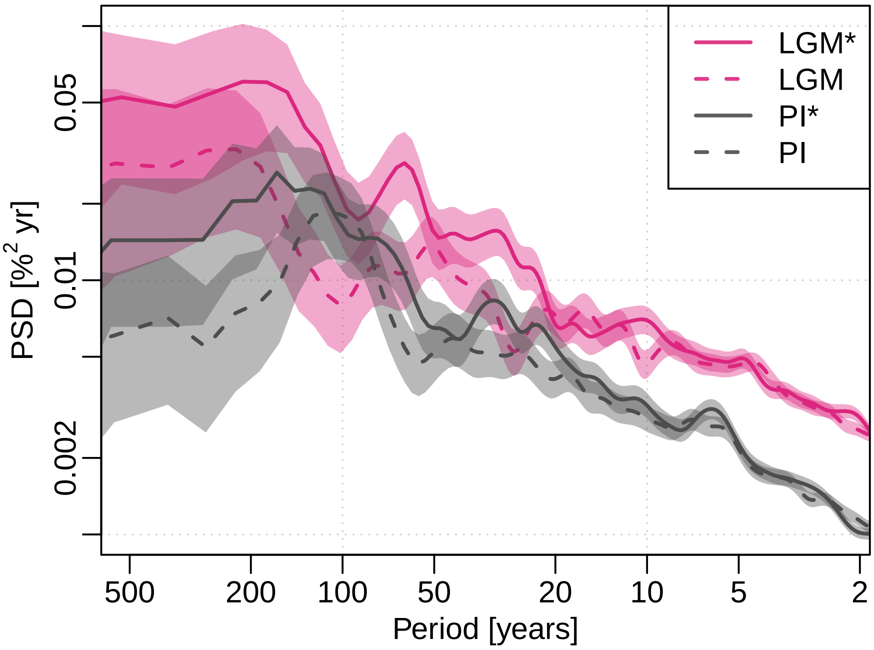

Figure S5. Power spectral density (PSD) of naturally forced and unforced global mean sea ice concentration as simulated by HadCM3 using Last Glacial and Pre-Industrial boundary conditions. The global mean sea ice concentration is defined as the percentage of the globe covered in sea ice.

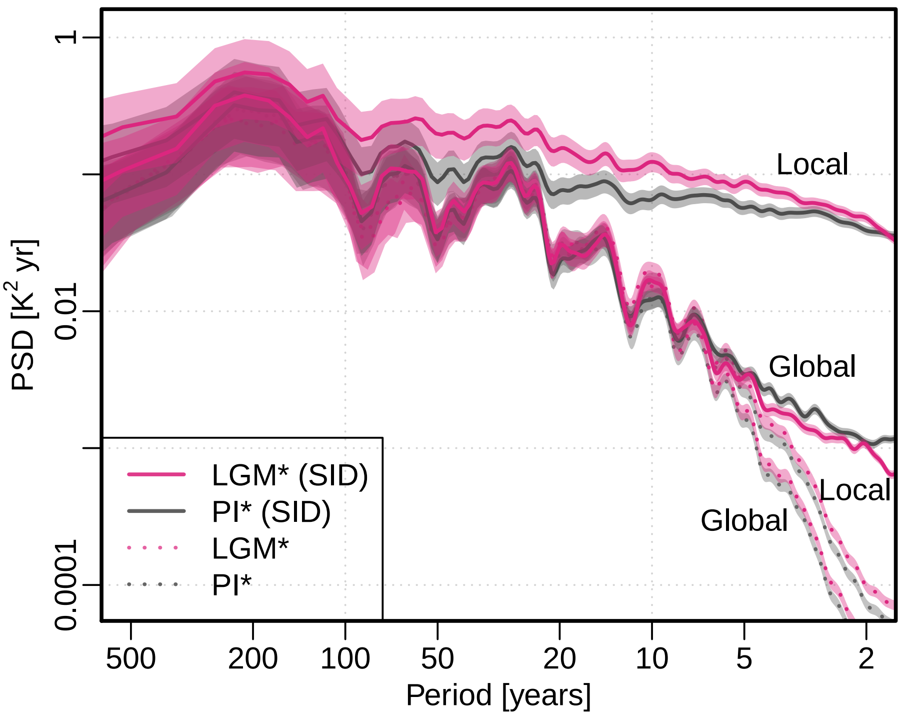

Figure S6. Global and local mean spectra of naturally forced surface air temperature as simulated by TransEBM with (solid lines) and without (dotted lines) time-varying sea ice dynamics (SID). TransEBM is a two-dimensional energy balance model with T42 resolution, as described by Ziegler and Rehfeld (2021) which draws on Zhuang et al. (2017). We run TransEBM with the same boundary conditions and time-varying forcing time series as the HadCM3 simulations, including the latitudinal-dependent volcanic forcing. Without loss of generality, we used the same constant CO2 values as in HadCM3 and neglected minor impacts from other greenhouse gases. The EBM is driven by yearly averaged solar and volcanic forcing. Dotted lines show the global and local mean spectra of the simulated temperature when sea ice extent is fixed. To mimic the sea ice dynamics in the two-dimensional model, we update the EBM's land-sea mask yearly based on the sea ice output from HadCM3 and repeat the simulations.

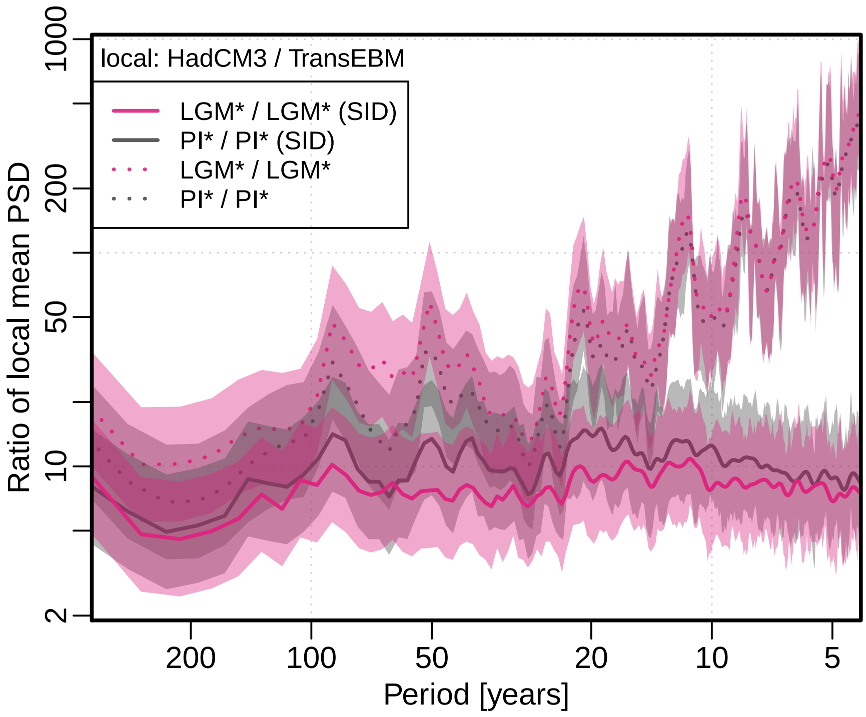

Figure S7. Ratio of HadCM3 (Figure 3) to TransEBM (Figure S6) local mean spectra (PSD) of naturally forced surface air temperature. LGM* / LGM* and PI* / PI* denote the ratios obtained from dividing the local mean spectrum of the naturally forced HadCM3 temperature by the one obtained from TransEBM with fixed sea ice. For the ratios of LGM* / LGM* (SID) and PI* / PI* (SID), time-varying sea ice dynamics in TransEBM was prescribed using the HadCM3 output. Hence, forming the ratio largely removes the linear response to naturally forcing and, for (SID), the contribution to variability from sea ice. The ratios therefore indicate the timescale-dependency of local variance simulated by HadCM3 that can be mainly attributed to internal dynamics excluding (solid lines) and including (dotted lines) sea ice dynamics. Shaded confidence intervals are computed from the F-distribution, based on the degrees of freedom of the spectral estimates.

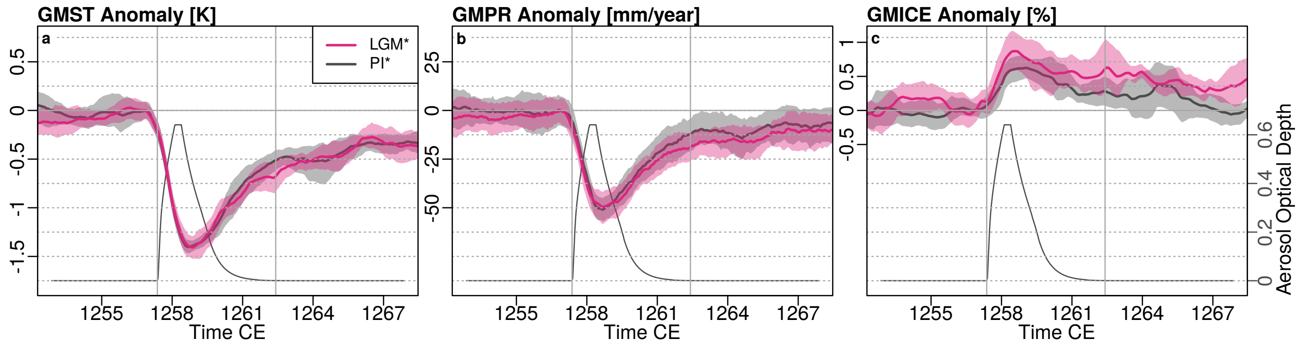

Figure S8. Superposed epoch analysis (see e.g., Sear et al. (1987); Brad Adams et al. (2003)) of globally averaged surface temperature (GMST, **a**), precipitation rate (GMPR, **b**), and sea ice concentration (GMICE, **c**) as simulated by HadCM3 using the reconstructed 1257 Samalas eruption. The lines represent the average value over all simulations in the LGM* and PI* state, and the shaded areas their respective ranges. The volcanic forcing from the Samalas eruption is shown in black. Anomalies are calculated against the three-year period before the eruption using the deseasonalized, detrended HadCM3 model output.

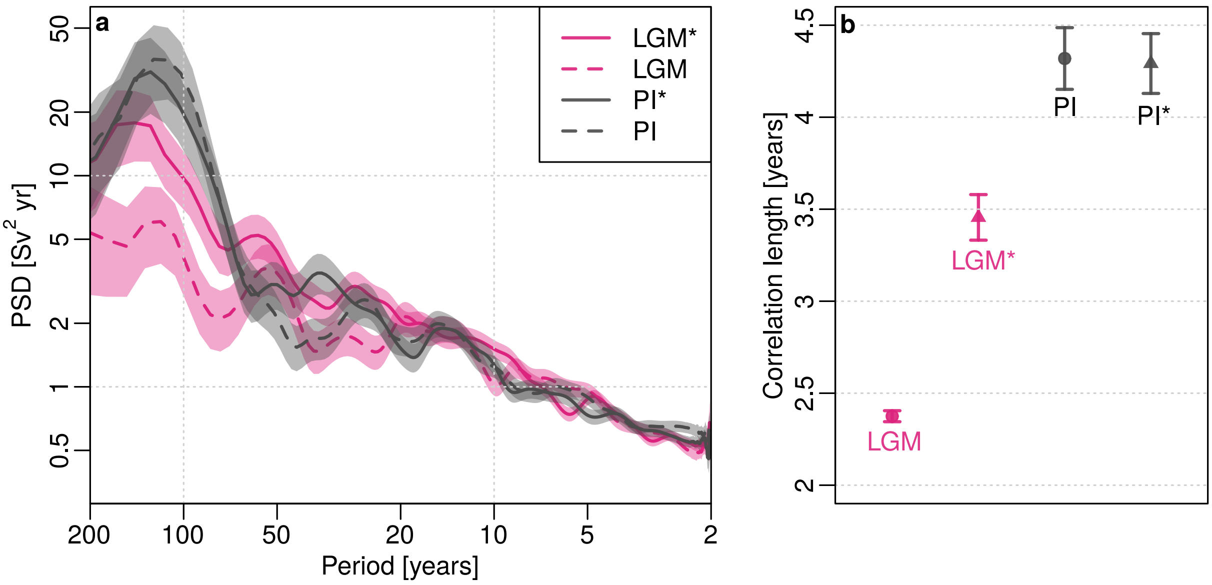

Figure S9. **a** Power spectral density (PSD) of the Atlantic Meridional Overturning Circulation (AMOC) strength from control and forced LGM and PI simulations using HadCM3. **b** Correlation length, defined as the lag at which the autocorrelation function first drops below 1/e and its standard error. Following Danabasoglu et al. (2012), we compute the AMOC strength as the maximum of the meridional ocean velocity field between 450 m and 2100 m depth and 20°N to 62.5°N at every timestep. Accordingly, the AMOC strength is given in Sv $= 10^6$ m^3 s^{-1}. The correlation length is an average of 3000 randomly sampled 100 year time slices of each state (1000 slices per run).

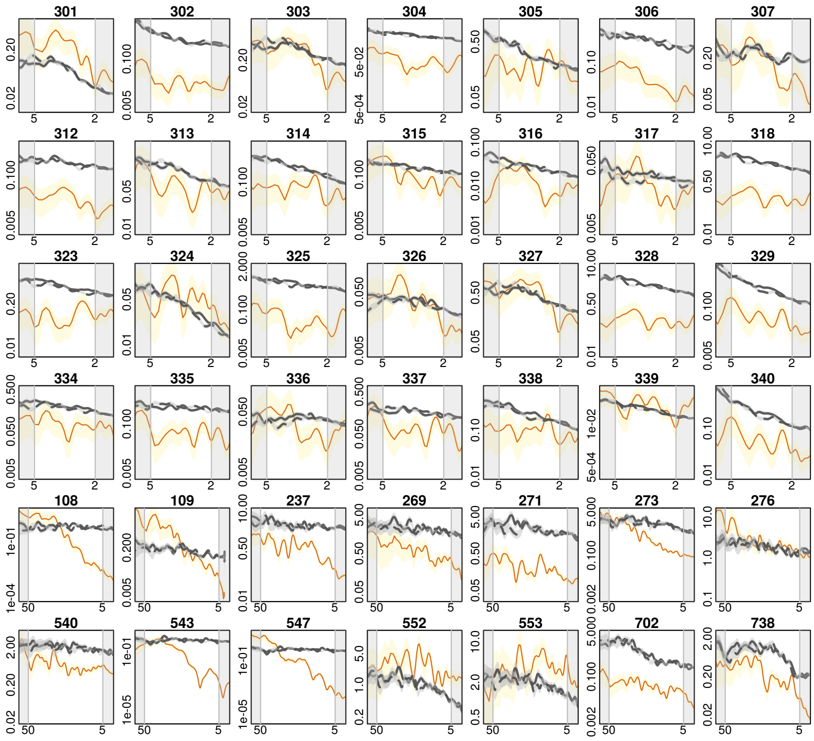

Figure S10. Temperature spectra from observations and proxy records (orange), and from HadCM3 simulations (grey) for the Pre-Industrial state, used for variance ratio estimates (Figure 4 of the main manuscript). The x-axis labels and background of each panel highlights the period (2-5 and 5-50 years) considered for timescale-dependent variance estimates. The y-axis denotes the power spectral density. Solid and dashed lines indicate forced and unforced runs. The title denotes the IDs from the separately uploaded dataset S1.

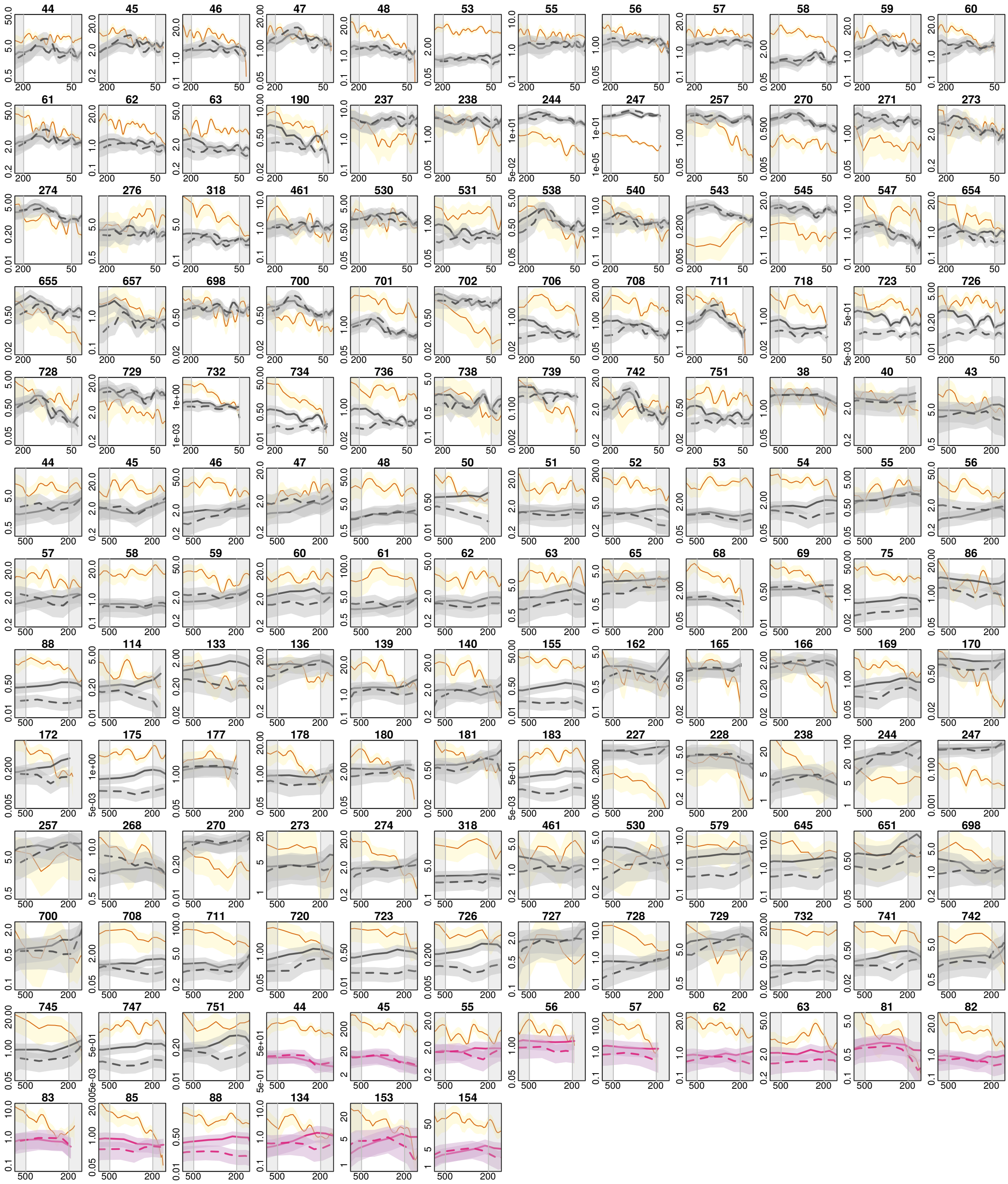

Figure S11. Same as Figure S10 but for multidecadal (50-200 years) and multicentennial (200-500 years) timescales. HadCM3 simulations under Last Glacial boundary conditions are shown in magenta.

Table S1. Boundary conditions of the HadCM3 simulation ensemble. Orbital parameters are internally calculated following (Berger, 1978) and Orography is taken from Singarayer and Valdes (2010) for 21 ka BP and 1850 CE. Greenhouse gas concentrations are taken from the protocols of the PMIP3 21ka and PI experiments (Schmidt et al., 2012). Vegetation is modeled with a 30-year timestep (Cox, 2001). Forced runs are driven by time-varying volcanic and solar (volc + sol) forcing as described in Table S2.

State	**Orography, Orb. Param.**	**CO_2, CH_4, N_2O**	**Forcing**	**#Runs**
Last Glacial Maximum (LGM)	21 ka BP	185ppm, 350ppb, 200ppb	–	3
Forced LGM (LGM*)	21 ka BP	185ppm, 350ppb, 200ppb	volc + sol	3
Pre-Industrial (PI)	1850 CE	280ppm, 650ppb, 270ppb	–	3
Forced PI (PI*)	1850 CE	280ppm, 650ppb, 270ppb	volc + sol	3

Table S2. Key specifications of the HadCM3 simulation ensemble. We provide the main references of the solar and volcanic forcing, whereby "-" indicates no forcing at all. The climate state defines the orography, orbital parameters, and greenhouse gas concentrations according to Table S1. The temporal resolution of each run is one month. The final column denotes the number of simulated years.

Name	Run ID	Climate state	Solar Forcing	Volcanic Forcing	Duration (yrs)
lgm1	xmzka	LGM	1365 W/m^2	–	1117
lgm2	xmzkd	LGM	1365 W/m^2	–	1066
lgm3	xmzki	LGM	1365 W/m^2	–	523
lgm4	xmzke	LGM*	Steinhilber et al. (2009); Wang, Lean, and Jr. (2005)	Crowley and Unterman (2013)	1064
lgm5	xmzkg	LGM*	Steinhilber et al. (2009); Wang et al. (2005)	Crowley and Unterman (2013)	1058
lgm6	xmzkh	LGM*	Steinhilber et al. (2009); Wang et al. (2005)	Crowley and Unterman (2013)	931
pi1	xnage	PI	1365 W/m^2	–	1055
pi2	xnagh	PI	1365 W/m^2	–	560
pi3	xnagb	PI	1365 W/m^2	–	1124
pi4	xnagd	PI*	Steinhilber et al. (2009); Wang et al. (2005)	Crowley and Unterman (2013)	1062
pi5	xnagf	PI*	Steinhilber et al. (2009); Wang et al. (2005)	Crowley and Unterman (2013)	1095
pi6	xnagg	PI*	Steinhilber et al. (2009); Wang et al. (2005)	Crowley and Unterman (2013)	1150